Supporting Information:

Non-Equilibrium Growth Processes to Glyceraldehyde and Glycerol as Building Blocks of Interstellar Sugars and Phospholipids

Xilin Bai,[1] Qi'ang Gong,[1] Jinghui Lu,[4] Jiuzhong Yang,[4] Yang Pan,[4] Zhenrong Sun,[1] Ralf I. Kaiser,[5*] Tao Yang[1,2,3*]

[1] *State Key Laboratory of Precision Spectroscopy, East China Normal University, Shanghai 200062, China*

[2] *Collaborative Innovation Center of Extreme Optics, Shanxi University, Taiyuan, Shanxi 030006, China*

[3] *State Key Laboratory of Radio Astronomy and Technology, Xinjiang Astronomical Observatory, Chinese Academy of Sciences, Urumqi, Xinjiang, 830011, China*

[4] *National Synchrotron Radiation Laboratory, University of Science and Technology of China, Hefei, Anhui 230029, China*

[5] *Department of Chemistry, University of Hawaii at Manoa, Honolulu, Hawaii 96822, United States*

[*]Corresponding Authors:

Ralf I. Kaiser, ralfk@hawaii.edu

Tao Yang, tyang@lps.ecnu.edu.cn

Supplementary Methods

1. Deposition ratio calibration of mixed ices

The deposition ratio of mixed ices was calibrated using a quadrupole mass spectrometer (QMS). Pure formaldehyde (H_2CO) and water (H_2O) ices were independently deposited to a thickness corresponding to a single interference fringe (~250 nm). During temperature-programmed desorption (TPD), the QMS monitored mass spectrometric signals. The results showed that H_2CO desorbed between 90 and 110 K, producing ion signals at *m/z* = 28 (CO^+), 29 (HCO^+), and 30 (H_2CO^+), while H_2O desorbed between 150 and 170 K, generating ion signals at *m/z* = 17 (OH^+) and 18 (H_2O^+). The integrated ion intensities were proportional to the number of deposited molecules, weighted by their respective ionization efficiencies. For mixed H_2CO–H_2O ices, three interference fringes were deposited under inlet pressures of $(1 \pm 0.1) \times 10^{-8}$ Torr for H_2CO and $(4 \pm 0.2) \times 10^{-8}$ Torr for H_2O. By quantifying the molecular abundances in the mixed ices relative to those from pure-component calibrations, the molecular ratio of H_2CO to H_2O in the mixed ices was determined to be 1:5.8 ± 0.9.

2. Ice thickness determination

Refractive indices of $n_{H2CO} = 1.33 \pm 0.04$ for solid formaldehyde and $n_{H2O} = 1.27 \pm 0.02$ for solid water were employed in Equation S1 to determine the ice thickness (d) based on laser interference fringes ($\lambda = 632.8$ nm, angle of incidence $\theta = 2°$).[1]

$$d = \frac{m\lambda}{2\sqrt{n_{mix}^2 - sin^2\theta}} \qquad \text{(S1)}$$

Here, the number of interference fringes (m) was extracted from intensity profiles, which captured the fringe pattern during ice growth. With three fringes observed, the total thickness of the H_2CO–H_2O ice mixture was calculated to be 743 ± 50 nm.

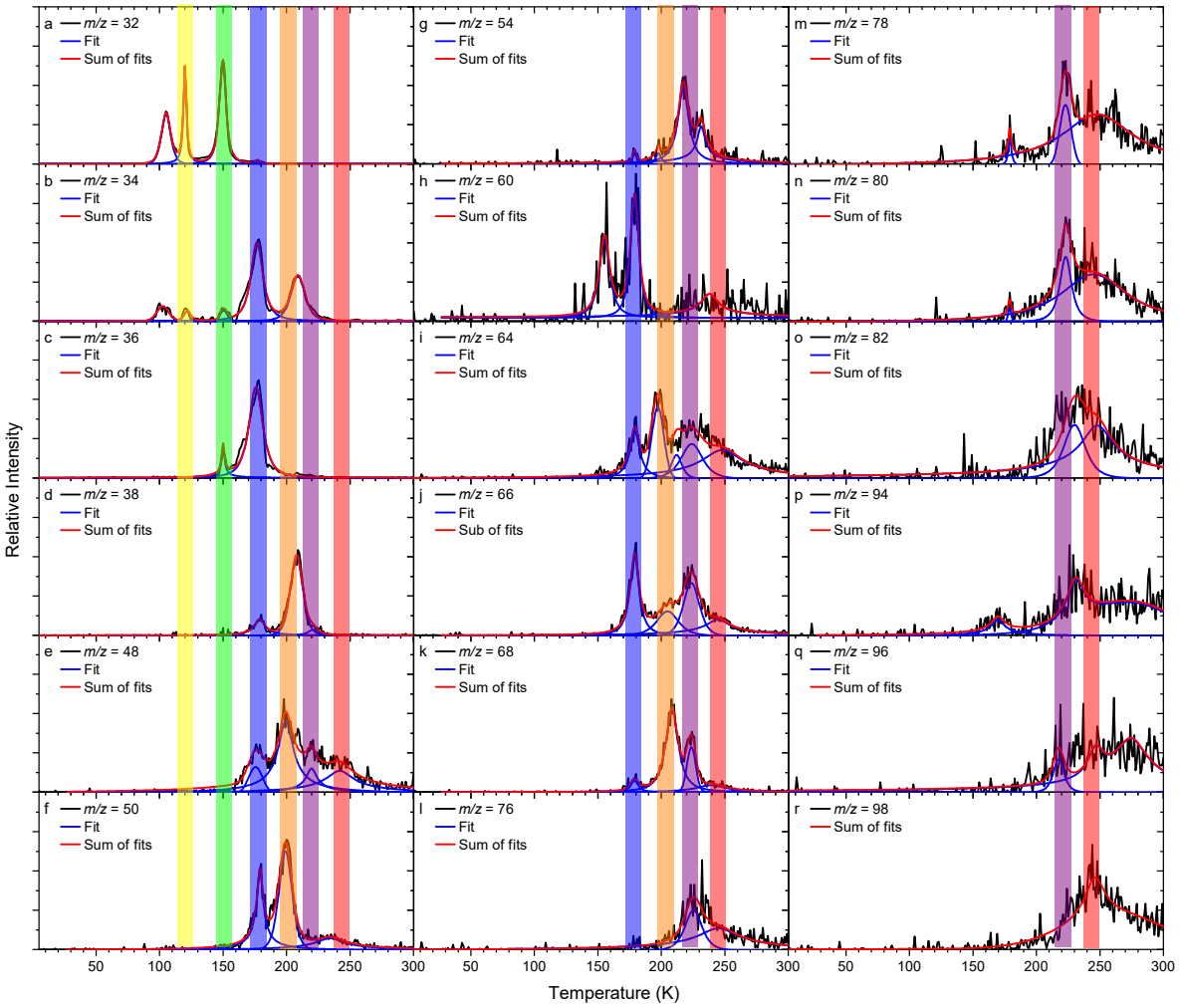

Figure S1. TPD spectra at distinct *m/z* observed in processed D_2CO–D_2O ices at the photoionization energy of 11.50 eV. Colored bars categorize molecular species that co sublime at specific temperatures, based on their dominant origin: fragmentation of a common parent molecule, volcanic effect associated with water ice, or co-sublimation with water. Blue lines represent data fitted with multiple Pearson peaks, and red lines indicate the total fit of deconvoluted profiles. The color sequence represents increasing sublimation temperatures: yellow (~120 K), green (~150 K), blue (~177 K), orange (~209 K), purple (~224 K), red (~246 K).

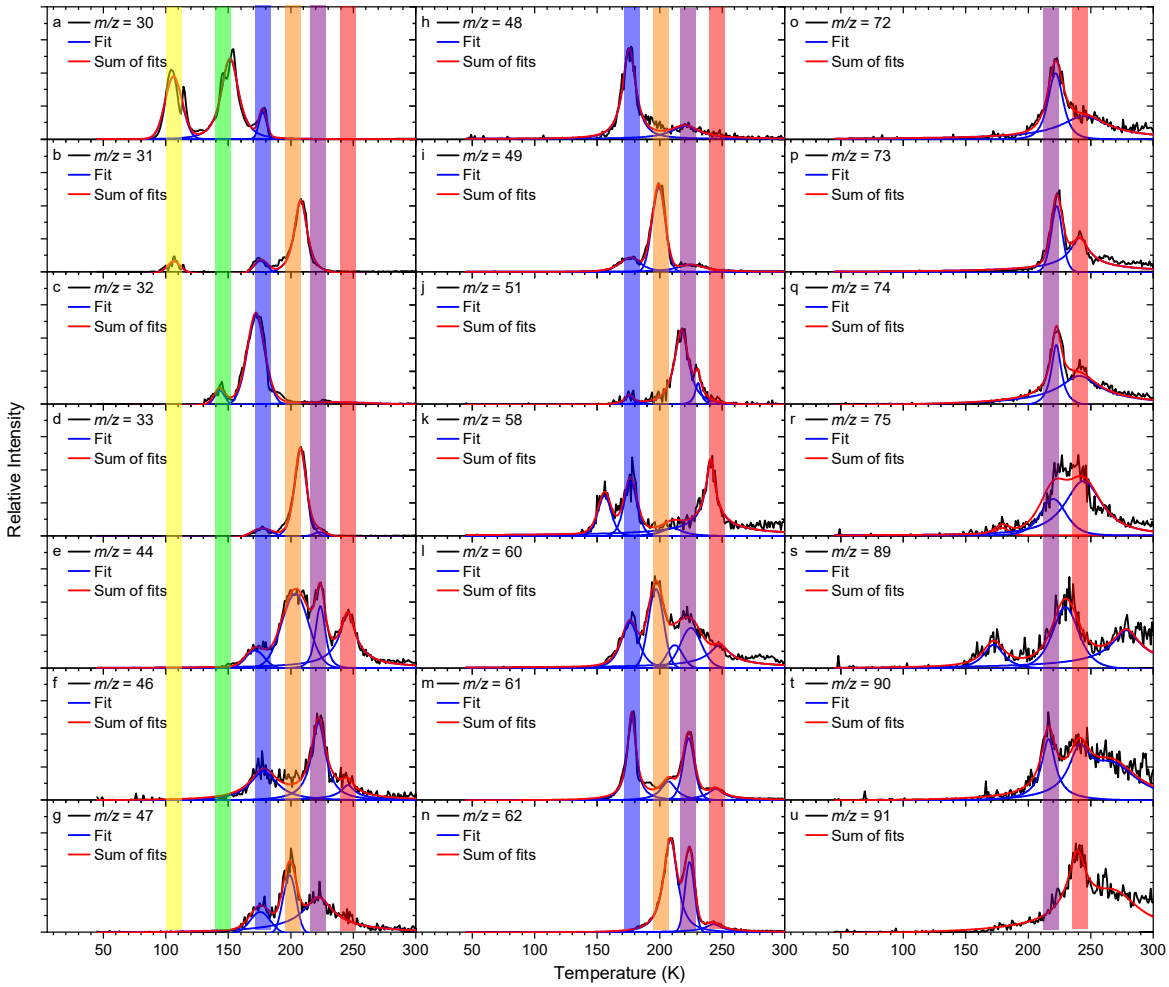

Figure S2. TPD spectra at distinct *m/z* observed in processed H_2CO–$H_2{}^{18}O$ ices at the photoionization energy of 11.50 eV. Colored bars categorize molecular species that co sublime at specific temperatures, based on their dominant origin: fragmentation of a common parent molecule, volcanic effect associated with water ice, or co-sublimation with water. Blue lines represent data fitted with multiple Pearson peaks, and red lines indicate the total fit of deconvoluted profiles. The color sequence represents increasing sublimation temperatures: yellow (~107 K), green (~144 K), blue (~177 K), orange (~209 K), purple (~224 K), red (~246 K).

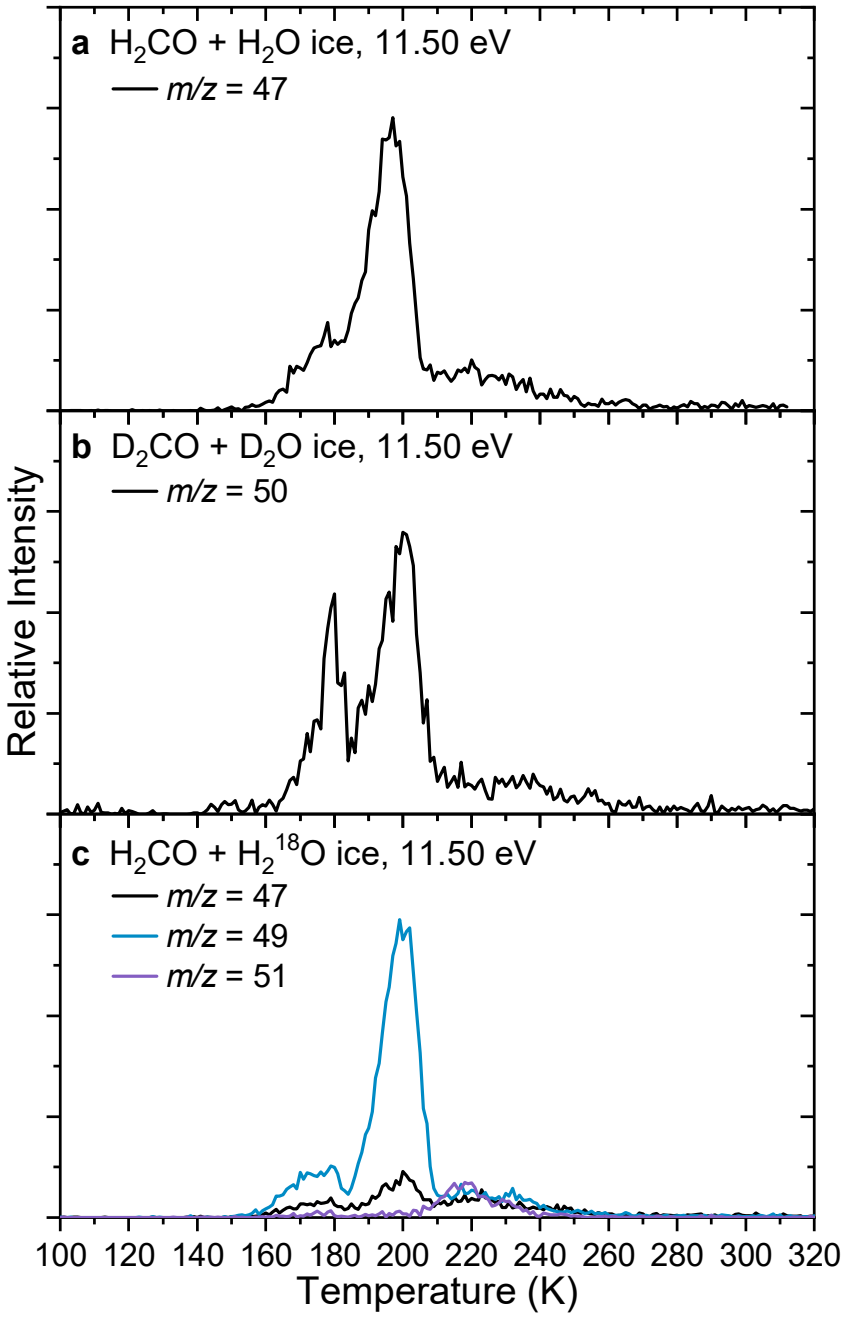

Figure S3. Ion signals during TPD of isotopically labeled formaldehyde–water ices as a function of temperature. TPD sublimation spectra for (**a**) *m/z* = 47 (H_2CO–H_2O), (**b**) *m/z* = 50 (D_2CO–D_2O), and (**c**) *m/z* = 47, 49 and 51 (H_2CO–$H_2{}^{18}O$) with irradiation obtained at the photoionization energy of 11.50 eV, respectively.

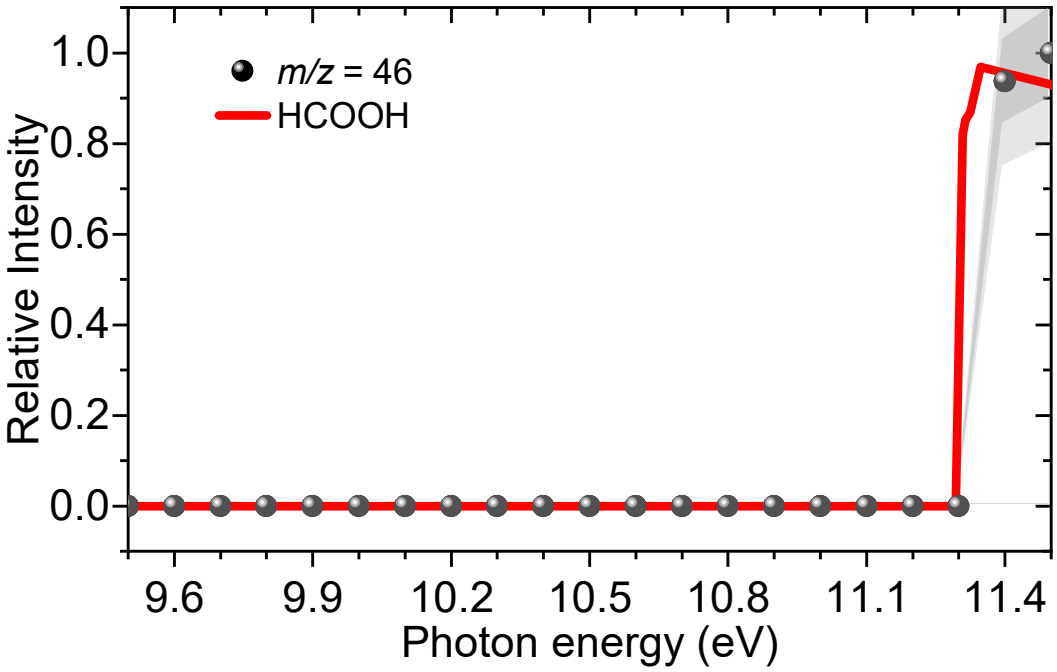

Figure S4. PIE curves linked to the formic acid ion ($HCOOH^+$, *m/z* = 46). Solid cycles represent experimental data, while the red line indicates the fitting of the reference PIE curve of formic acid.[2] The dark-gray and light-gray shaded regions indicate the 1σ and 2σ standard deviations of the PIE curve (averaged across individual scans), respectively.

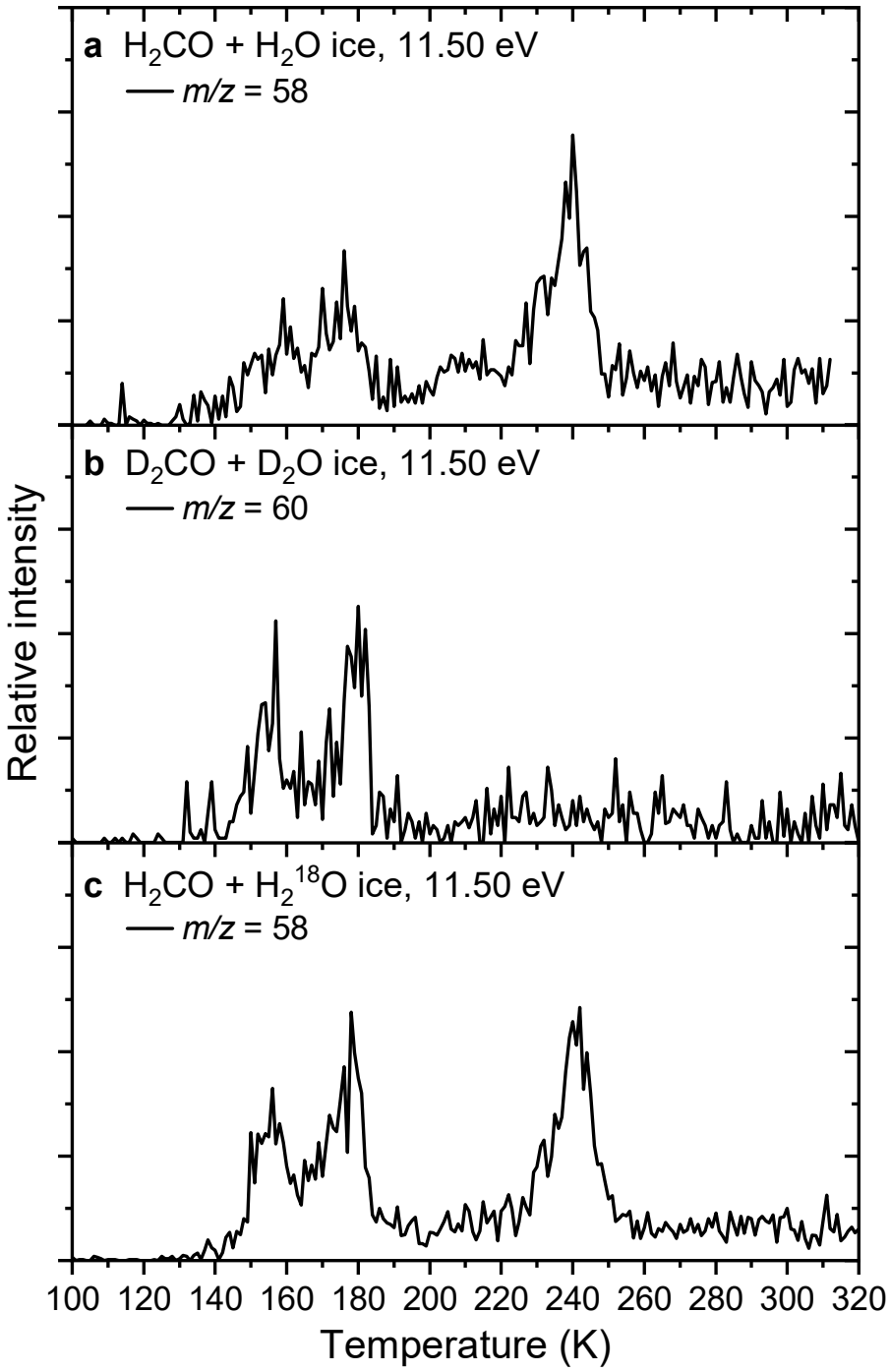

Figure S5. Ion signal during TPD of isotopically labeled formaldehyde–water ices as a function of temperature. TPD sublimation spectra for (**a**) *m/z* = 58 (H_2CO–H_2O), (**b**) *m/z* = 60 (D_2CO–D_2O), and (**c**) *m/z* = 58 (H_2CO–$H_2{}^{18}O$) with irradiation obtained at the photoionization energy of 11.50 eV, respectively.

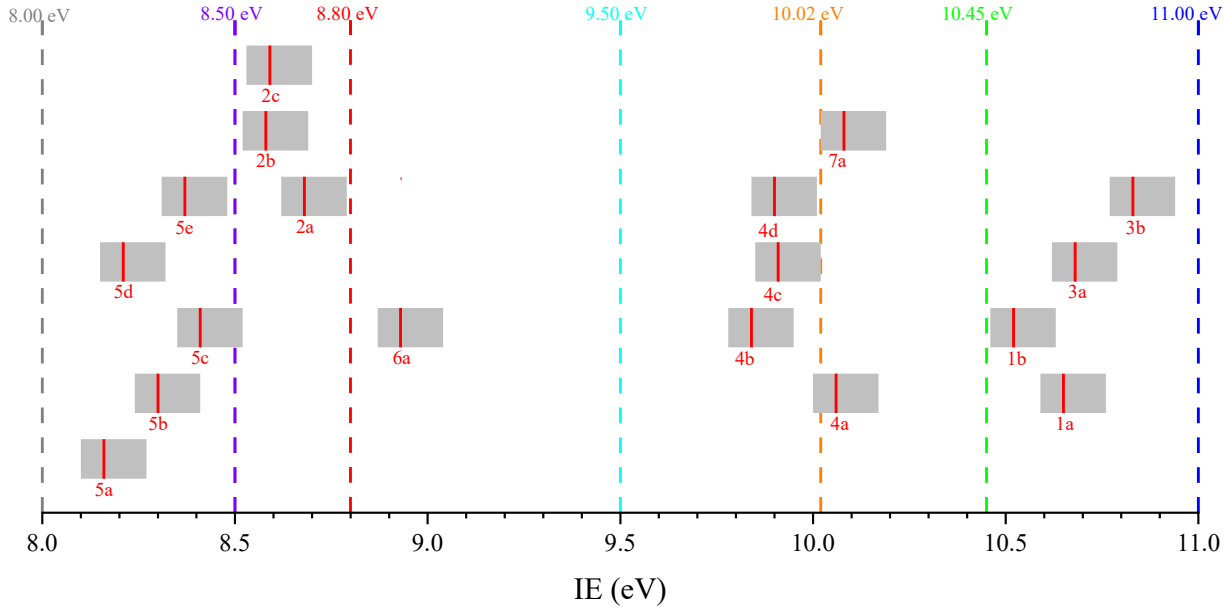

Figure S6. Adiabatic ionization energies (AIEs) of $C_2H_4O_2$ isomers. Computed AIEs of $C_2H_4O_2$ isomers (solid red lines) along with error limits are adapted from Kleimeier *et al.*[3] The numbers 1a to 7a correspond to isomers 1a to 7a in Table S2.

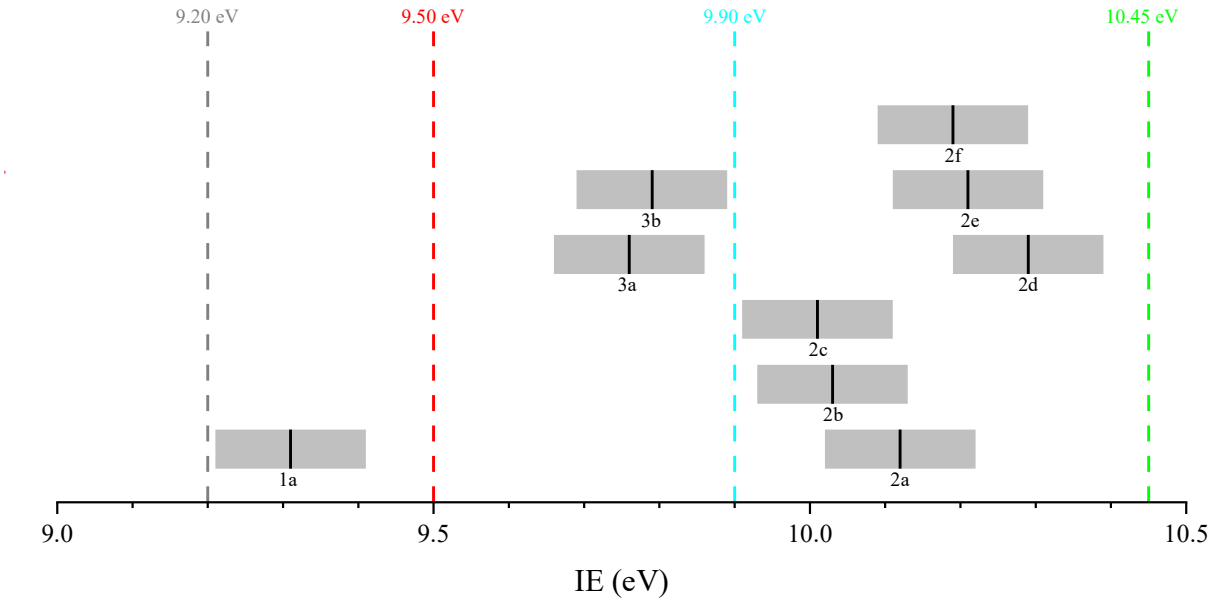

Figure S7. AIEs of $C_2H_6O_2$ isomers. Computed AIEs of $C_2H_6O_2$ isomers (solid black lines) along with error limits are adapted from Zhu *et al*.[4] The numbers 1a to 3b correspond to isomers 1a to 3b in Table S3.

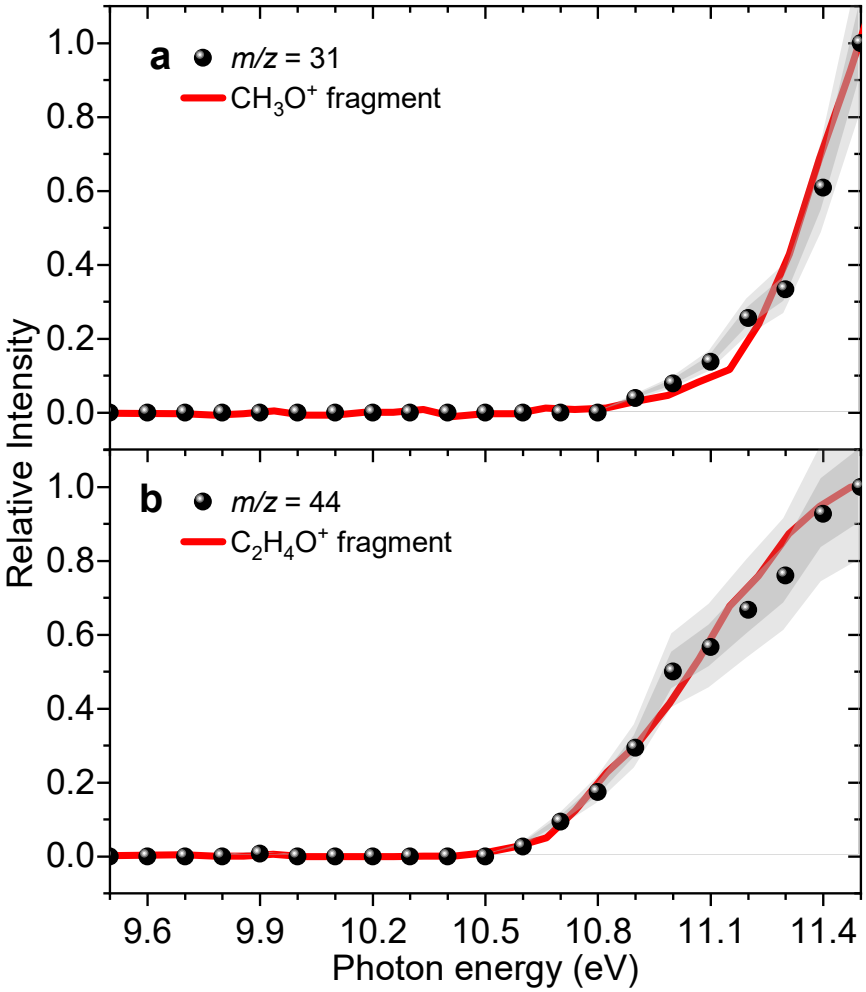

Figure S8. PIE curves for species linked to fragment ions of ethylene glycol. Fragment ions (**a**) CH_3O^+ (*m/z* = 31) and (**b**) $C_2H_4O^+$ (*m/z* = 44) are associated with ethylene glycol, respectively. Solid cycles represent experimental data, while red lines indicate the fitting of reference PIE curves.[5] The dark-gray and light-gray shaded regions indicate the 1σ and 2σ standard deviations of the PIE curve (averaged across individual scans), respectively.

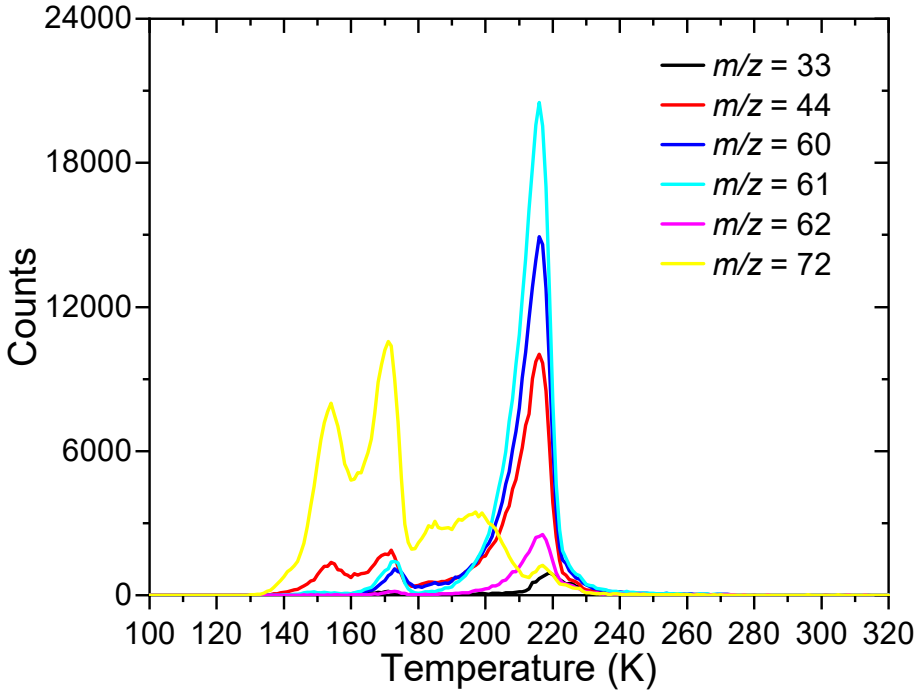

Figure S9. TPD spectra of glyceraldehyde. TPD spectra recorded in pure glyceraldehyde ice at the photoionization energy of 11.50 eV.

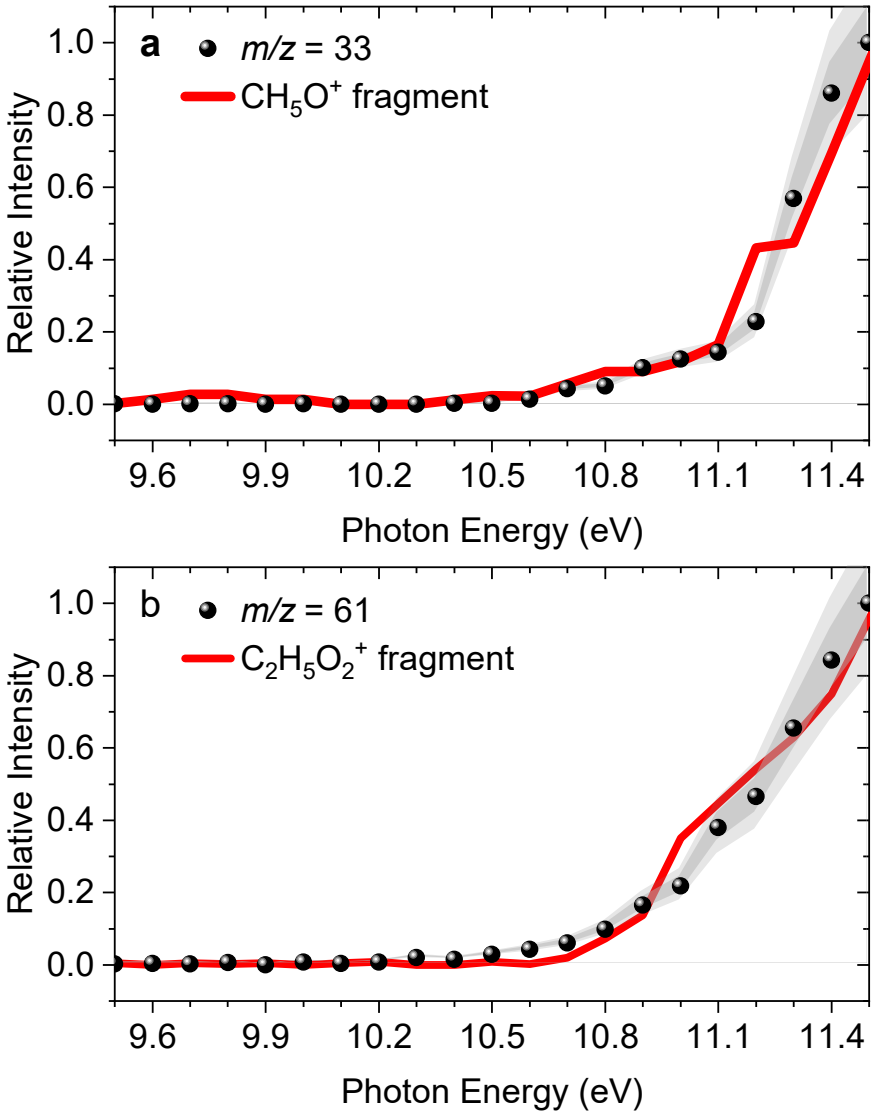

Figure S10. PIE curves for species linked to fragment ions of glyceraldehyde. Fragment ions (**a**) CH_5O^+ (*m/z* = 33) and (**b**) $C_2H_5O_2^+$ (*m/z* = 61) are associated with glyceraldehyde, respectively. Solid cycles represent experimental data, while red lines indicate the fitting of reference PIE curves. The dark-gray and light-gray shaded regions indicate the 1σ and 2σ standard deviations of the PIE curve (averaged across individual scans), respectively.

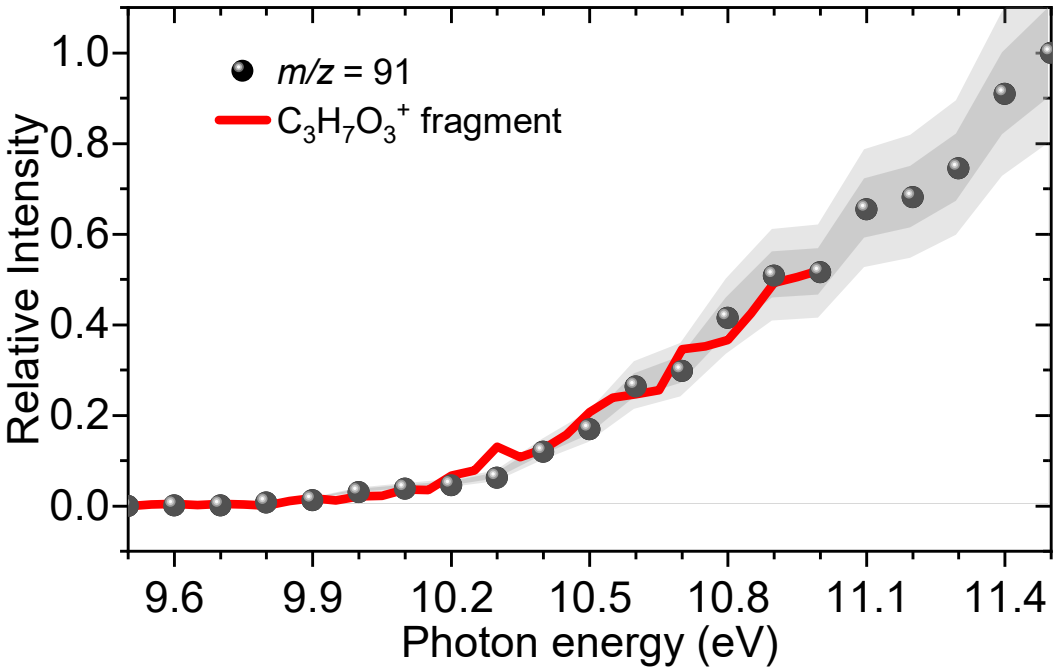

Figure S11. PIE curves linked to the fragment ion $C_3H_7O_3^+$ (*m/z* = 91) associated with (methoxymethoxy)methanol. Solid cycles represent experimental data, while the red line indicate the fitting of the reference PIE curve of (methoxymethoxy)methanol.[6] The dark-gray and light-gray shaded regions indicate the 1σ and 2σ standard deviations of the PIE curve (averaged across individual scans), respectively.

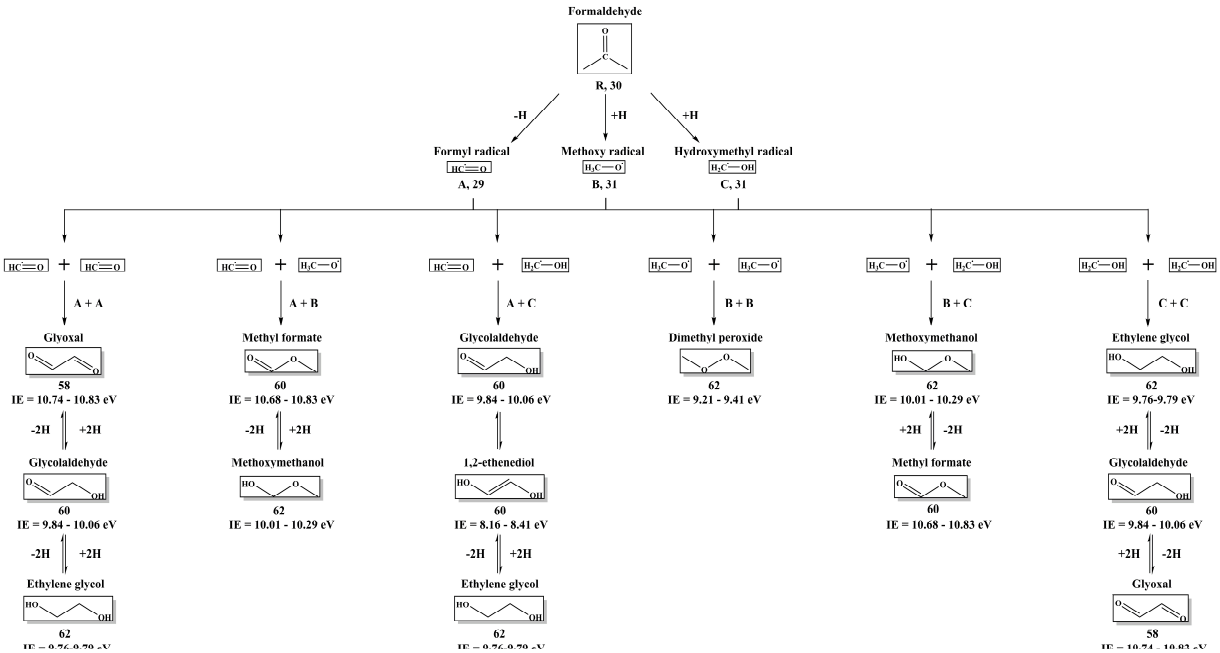

Figure S12. Radical-radical reaction scheme. Proposed radical-radical reaction scheme for $C_2H_4O_2$ and $C_2H_6O_2$ isomers.

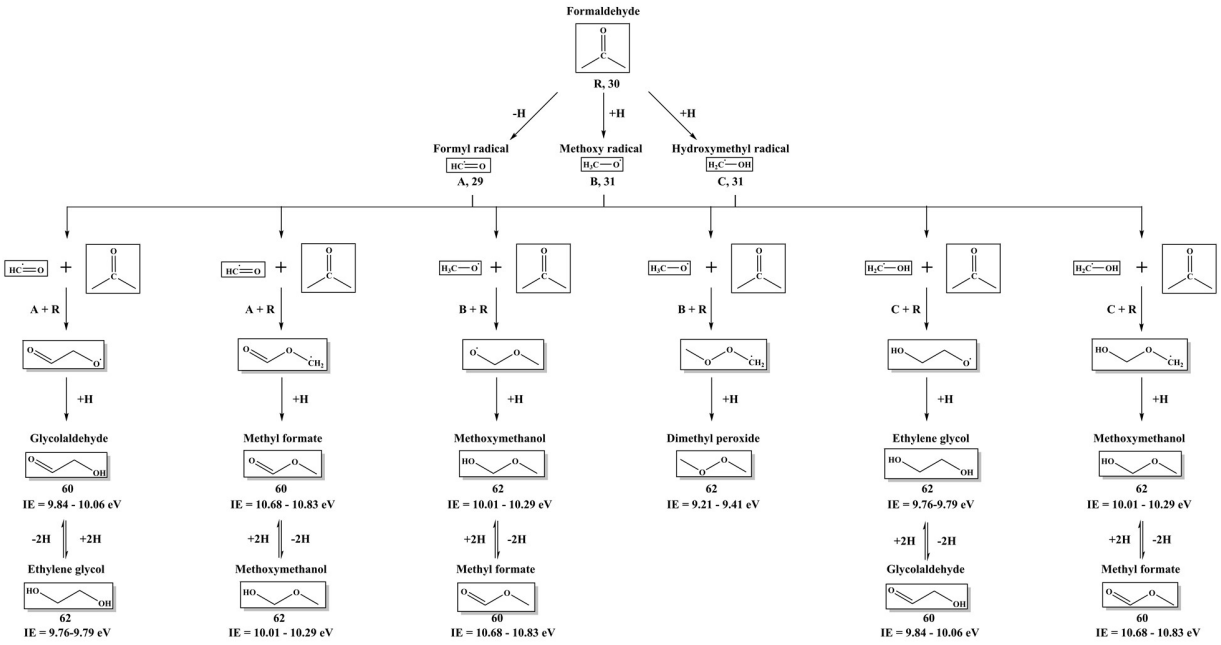

Figure S13. Molecule-radical reaction scheme. Proposed molecule-radical reaction scheme for $C_2H_4O_2$ and $C_2H_6O_2$ isomers.

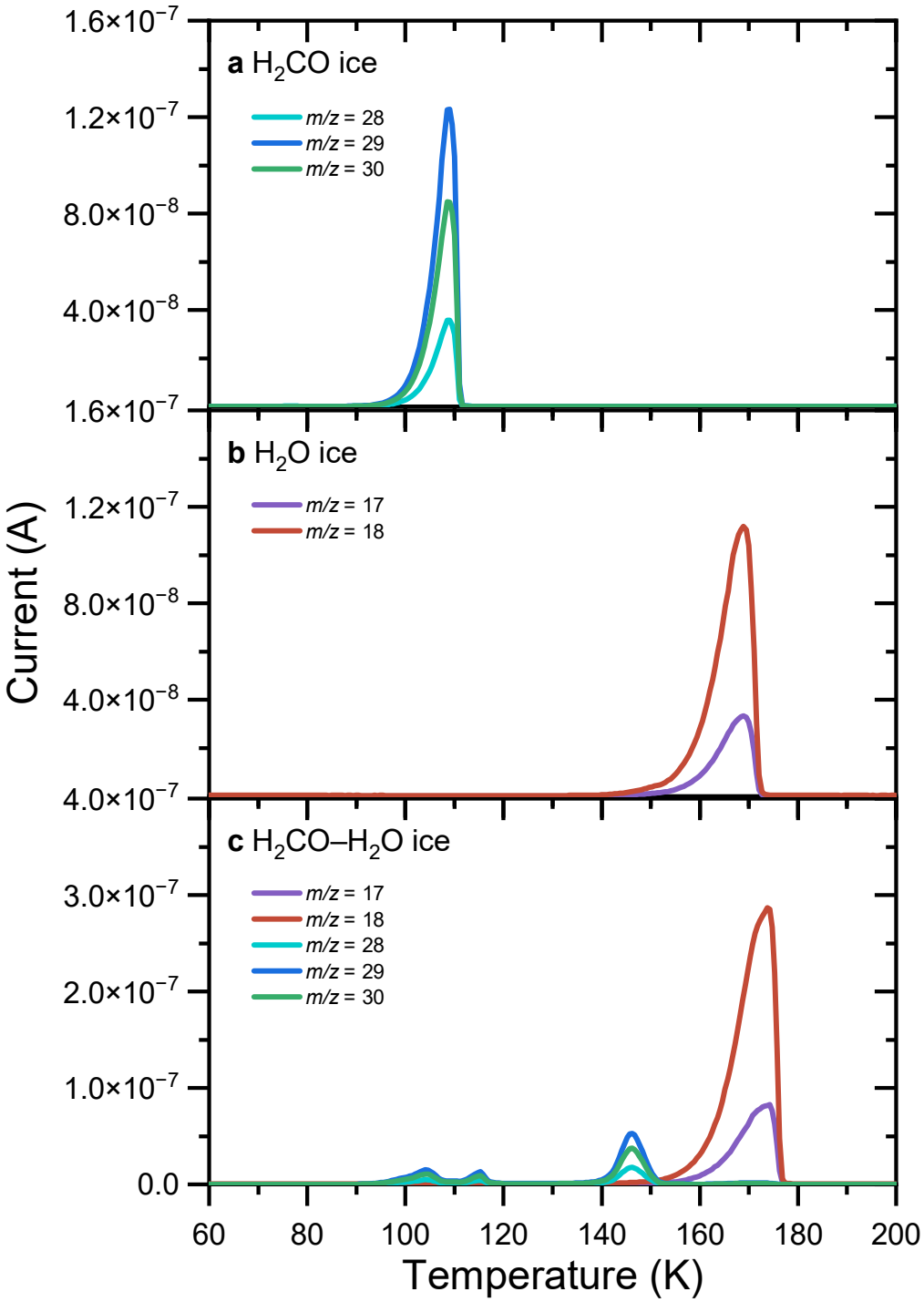

Figure S14. Ion currents at distinct *m*/*z* obtained via EI-QMS in the TPD phase. Ion currents of species released into the gas phase in (**a**) pure H_2CO, (**b**) pure H_2O, and (**c**) H_2CO–H_2O mixed ices, respectively.

Table S1. Molecular formula and corresponding mass-to-charge ratios of products identified in the irradiated formaldehyde–water isotopologue ices (H_2CO–H_2O, D_2CO–D_2O, and H_2CO–$H_2{}^{18}O$) during the TPD phase using SVUV-PI-ReToF-MS.

H_2CO–H_2O		D_2CO–D_2O		H_2CO–$H_2{}^{18}O$	
Formula	*m/z*	Formula	*m/z*	Formula	*m/z*
Products with a single carbon atom					
CH_3OH	32	CD_3OD	36	CH_3OH	32
HCOOH	46	DCOOD	48	$HCO^{18}OH$	48
$CH(OH)_3$	64	$CD(OD)_3$	68	$CH(OH)(^{18}OH)_2$	68
Products with two carbon atoms					
$C_2H_2O_2$	58	$C_2D_2O_2$	60	$C_2H_2O_2$	58
$C_2H_4O_2$	60	$C_2D_4O_2$	64	$C_2H_4O_2$	60
$C_2H_5O_2$	61	$C_2D_5O_2$	66	$C_2H_5O_2$	61
$C_2H_6O_2$	62	$C_2D_6O_2$	68	$C_2H_6O_2$	62
Products with three carbon atoms					
$C_3H_6O_3$	90	$C_3D_6O_3$	96	$C_3H_6O_3$	90
$C_3H_8O_3$	92	$C_3D_8O_3$	100	$C_3H_8O_3$	92

Table S2. The calculated AIEs of $C_2H_4O_2$ isomers adapted from Kleimeier *et al.*[3] AIE ranges were corrected for combined error limits, which were determined to be –0.06/+0.11 eV (IE_{corr1}) and the thermal and Stark effect by –0.02 eV (IE_{corr2}).[7]

Isomers	IE_{calc} **(eV)**	IE_{corr1} **(eV)**	IE_{corr2} **(eV)**
anti-acetic acid (1a)	10.65	10.59–10.76	10.57–10.74
anti-acetic acid (1b)	10.52	10.46–10.63	10.44–10.61
syn, syn-1,1-ethenediol (2a)	8.68	8.62–8.79	8.60–8.77
syn, anti-1,1-ethenediol (2b)	8.58	8.52–8.69	8.50–8.67
anti, anti-1,1-ethenediol (2c)	8.59	8.53–8.70	8.51–8.68
anti-methyl formate (3a)	10.68	10.62–10.79	10.60–10.77
syn-methyl formate (3b)	10.83	10.77–10.94	10.75–10.92
syn, *syn*-glycolaldhyde (4a)	10.06	10.00–10.17	9.98–10.15
syn, *anti*-glycolaldehyde (4b)	9.84	9.78–9.95	9.76–9.93
anti, *anti*-glycolaldehyde (4c)	9.91	9.85–10.02	9.83–10.00
anti, *gauche*-glycolaldehyde (4d)	9.90	9.84–10.01	9.82–9.99
E-anti-anti-1,2-ethenediol(5a)	8.16	8.10–8.27	8.08–8.25
E-syn-anti-1,2-ethenediol (5b)	8.30	8.24–8.41	8.22–8.39
E-syn-syn-1,2-ethenediol (5c)	8.41	8.35–8.52	8.33–8.50
Z-anti-anti-1,2-ethenediol (5d)	8.21	8.15–8.32	8.13–8.30
Z-syn-anti-1,2-ethenediol(5e)	8.37	8.31–8.48	8.29–8.46
Oxiran-2-ol (6a)	8.93	8.87–9.04	8.85–9.02
1,3-Dioxetane (7a)	10.08	10.02–10.19	10.00–10.17

Table S3. The calculated AIEs of $C_2H_6O_2$ isomers adapted from Zhu *et al*.[4] AIE ranges were corrected for combined error limits, which were determined to be –0.10/+0.10 eV (IE_{corr1}) and the thermal and Stark effect by –0.02 eV (IE_{corr2}).

Isomers	IE_{calc} **(eV)**	IE_{corr1} **(eV)**	IE_{corr2} **(eV)**
Dimethyl peroxide (1a)	9.31	9.21–9.41	9.19–9.39
1-*gauche*-Methoxymethanol (2a)	10.12	10.02–10.22	10.00–10.20
2-*gauche*-Methoxymethanol (2b)	10.03	9.93–10.13	9.91–10.11
3-*gauche*-Methoxymethanol (2c)	10.01	9.91–10.11	9.89–10.09
1-*eclipsed*-Methoxymethanol (2d)	10.29	10.19–10.39	10.17–10.37
2-*eclipsed*-Methoxymethanol (2e)	10.21	10.11–10.31	10.09–10.29
3-*eclipsed*-Methoxymethanol (2f)	10.19	10.09–10.29	10.07–10.27
gauche-Ethylene glycol (3a)	9.76	9.66–9.86	9.64–9.84
anti-Ethylene glycol (3b)	9.79	9.69–9.89	9.67–9.87

Table S4. Energies, geometries, and frequencies used in calculating the AIE of 1,1-ethanediol ($CH_3CH(OH)_2$).

No.	Name	Energies (a.u.)	Atom	X (Å)	Y (Å)	Z (Å)	ν (cm^{-1})	T1 diag.
0	$CH_3CH(OH)_2$_neutral	ZPE(ωB97X-D/def2-TZVP)=0.0856885 E(ωB97X-D/def2-TZVP)=−230.2971464 E(UCCSD(T)/aug-cc-pVDZ)=−229.7517734 E(UCCSD(T)/aug-cc-pVTZ)=−229.9584214	C H H H C H O H O H	1.399480 1.452466 1.926890 1.884825 −0.046072 −0.118705 −0.673074 −1.589424 −0.708367 −0.624975	−0.036220 −0.027595 0.831919 −0.942322 −0.002837 −0.003452 −1.141398 −1.134496 1.172753 1.259444	−0.082747 −1.173059 0.307245 0.275123 0.359385 1.450522 −0.175553 0.106410 −0.029883 −0.982577	 239.9, 323.8, 376.9 403.2, 496.8, 585.9 876.6, 960.6, 1054.4 1101.8, 1157.1, 1286.5 1313.5, 1401.8, 1424.8 1473.3, 1489.1, 1500.4 3050.9, 3056.9, 3136.1 3156.7, 3860.6, 3885.4 	0.0123
1	$CH_3CH(OH)_2$_cation	ZPE(ωB97X-D/def2-TZVP)=0.0846417 E(ωB97X-D/def2-TZVP)=−229.91516 E(UCCSD(T)/aug-cc-pVDZ)=−229.3679923 E(UCCSD(T)/aug-cc-pVTZ)=−229.5691634	C H H H C H O H O H	1.453326 1.454281 2.008748 1.946631 0.067954 −0.022185 −0.777758 −1.576267 −0.768419 −0.569468	−0.048952 −0.020061 0.800046 −0.962593 −0.023409 −0.071403 −0.969066 −1.158408 1.041994 1.263162	−0.115067 −1.205055 0.281772 0.214658 0.425070 1.506497 −0.231225 0.295443 −0.019275 −0.949338	 234.5, 374.2, 433.7 515.2, 571.3, 598.6 717.9, 885.2, 1033.7 1056.2, 1150.8, 1201.1 1288.5, 1343.7, 1421.6 1461.4, 1476.7, 1493.0 3062.2, 3149.1, 3156.5 3172.1, 3662.4, 3693.9 	0.0167

E(CCSD(T)/CBS) = [E(UCCSD(T)/aug-cc-pVTZ) – ($2.5^3/3.5^3$) E(UCCSD(T)/aug-cc-pVDZ)] / [1 – ($2.5^3/3.5^3$)] + 0.975 ZPE(ωB97X-D/def2-TZVP)

AIE[$CH_3CH(OH)_2$] = E(CCSD(T)/CBS)[$CH_3CH(OH)_2$_cation] – E(CCSD(T)/CBS)[$CH_3CH(OH)_2$_neutral] = 10.65 eV

Table S5. List of experiments.

#	Precursors	Electron dose	Photoionization Energy (eV)
1	H_2CO–H_2O	0 nA, blank	11.50
2	H_2CO–H_2O	100 nA, 30 min	11.50
3	D_2CO–D_2O	100 nA, 30 min	11.50
4	H_2CO–$H_2{}^{18}O$	100 nA, 30 min	11.50
5	H_2CO–H_2O	100 nA, 30 min	PIE_1 (9.50–11.50)
6	H_2CO–H_2O	100 nA, 30 min	PIE_2 (9.50–11.50)
7	H_2CO–H_2O	100 nA, 30 min	PIE_3 (9.50–11.50)

Table S6. Values used to determine the irradiation dose per molecule.

Initial kinetic energy of the electrons, E_{init}		5 keV
Irradiation current, I		100 ± 10 nA
Irradiation time, t		1800 s
Total number of electrons		$(5.6 \pm 0.6) \times 10^{13}$
Average kinetic energy of backscattered electrons, E_{bs}*		3.3 ± 0.3 keV
Fraction of backscattered electrons, f_{bs}*		0.36 ± 0.04
Average kinetic energy of transmitted electrons, E_{trans}*		0 keV
Fraction of transmitted electrons, f_{trans}*		0
Average penetration depth, l*		324 ± 32 nm
Density of the ice, ρ		0.86 g cm^{-3}
Dose per molecule	H_2CO	8.6 eV
	H_2O	5.2 eV

Note:

* Parameters obtained using the CASINO software v2.42.[8]

Supplementary References

(1) Bouilloud, M.; Fray, N.; Bénilan, Y.; Cottin, H.; Gazeau, M. C.; Jolly, A. Bibliographic review and new measurements of the infrared band strengths of pure molecules at 25 K: H_2O, CO_2, CO, CH_4, NH_3, CH_3OH, HCOOH and H_2CO. *MNRAS* **2015**, *451*, 2145-2160.
(2) Fujimoto, M.; Tanaka, H.; Marinho, R.; Medina, A.; Prudente, F.; Homem, M. Cross Sections and Asymmetry Parameters for Formic Acid in the Vacuum-Ultraviolet Energy Range. *J. Phys. Chem. A* **2020**, *124*, 6478-6485.
(3) Kleimeier, N. F.; Eckhardt, A. K.; Kaiser, R. I. Identification of Glycolaldehyde Enol (HOHC═CHOH) in Interstellar Analogue Ices. *J. Am. Chem. Soc.* **2021**, *143*, 14009-14018.
(4) Zhu, C.; Frigge, R.; Bergantini, A.; Fortenberry, R. C.; Kaiser, R. I. Untangling the Formation of Methoxymethanol (CH_3OCH_2OH) and Dimethyl Peroxide (CH_3OOCH_3) in Star-forming Regions. *Astrophys. J.* **2019**, *881*.
(5) Wang, H.; Guan, J.; Gao, J.; Li, Y.; Zhang, J.; Shan, X.; Wang, Z. Discriminating between the dissociative photoionization and thermal decomposition products of ethylene glycol by synchrotron VUV photoionization mass spectrometry and theoretical calculations. *Phys. Chem. Chem. Phys.* **2022**, *24*, 26915-26925.
(6) Gong, Q. a.; Bai, X.; Lu, J.; Yang, J.; Pan, Y.; Sun, Z.; Kaiser, R. I.; Yang, T. Formation of Polyoxymethylenes in Extraterrestrial Ice Analogs of Formaldehyde Exposed to Ionizing Radiation. *Astrophys. J.* **2025**, *994*, 70.
(7) Zhu, C.; Wang, H.; Medvedkov, I.; Marks, J.; Xu, M.; Yang, J.; Yang, T.; Pan, Y.; Kaiser, R. I. Exploitation of synchrotron radiation photoionization mass spectrometry in the analysis of complex organics in interstellar model ices. *J. Phys. Chem. Lett.* **2022**, *13*, 6875-6882.
(8) Drouin, D.; Couture, A. R.; Joly, D.; Tastet, X.; Aimez, V.; Gauvin, R. CASINO V2.42: a fast and easy-to-use modeling tool for scanning electron microscopy and microanalysis users. *Scanning* **2007**, *29*, 92-101.